Polarization states of diffracted light
Changes accompanying fiber activation

J.S. Chen, R.J. Baskin,* R. James Baskin,* K. Burton, S. Shen,‡ and Y. Yeh‡
Departments of Zoology* and Applied Science‡ and Group in Biophysics, University of California, Davis, California

ABSTRACT Measurement of the state of optical polarization of light diffracted from single, skinned and intact fibers of anterior tibialis muscle from *Rana pipiens* revealed a dependence upon rigor, activation, and sarcomere length (SL) change. Changes in total birefringence, Δn_T, and differential field ratio value, r_T, were determined.

In a relaxed, skinned fiber the total birefringence value, Δn_T, decreases as sarcomere length is increased from 2.1 μm to ~2.8–3.0 μm. From there it increases significantly to a value of $\sim 1.8 \times 10^{-3}$ at a sarcomere length of 3.6 μm. The differential field ratio, r_T, also shows a biphasic response to increasing sarcomere length, first exhibiting a rapid decrease over shorter SL and leveling out after the SL is beyond 3.0 μm. In comparison, relaxed intact fibers change substantially less upon sarcomere length change, showing little change in birefringence and a small bi-phasic change in r_T.

Skinned fibers were activated using a solution that has the same ionic strength as the relaxing solution and allows repeatable, and sustained activation. A decrease in both Δn_T and r_T was observed upon fiber activation. The decrease in Δn_T and r_T was slightly larger at shorter sarcomere lengths than at longer lengths. Relaxed fibers placed in rigor showed changes in Δn_T and r_T similar to those observed in activated fibers.

These results are consistent with the hypothesis that, after activation, a significant portion of the thick filament cross-bridges rotate towards the actin filament resulting in redistribution of the interfilament mass content. They are also consistent with an average orientation of crossbridges in the overlap region different from that in the non-overlap region.

I. INTRODUCTION

Complete characterization of the state of optical polarization of light diffracted from single fibers requires the determination of both the total birefringence, Δn_T, and differential field ratio (DFR), r_T. (For a more complete discussion see Yeh and Baskin, 1988). We have published evidence (Baskin et al., 1986) linking changes in these parameters with changes in crossbridge configuration. In the present investigation we are extending our measurements of the complete state of polarization of the diffracted light to characterize the chemically activated, skinned fiber. We also include a more extensive determination of the changes in the state of polarization accompanying passive stretch of both skinned and intact fibers. The rationale for comparing skinned fibers with intact fibers is that the former does not allow isovolumic stretch as does the latter. Thus the contribution of filament separation distance to the measured state of polarization can be characterized.

Address correspondence to Dr. R.J. Baskin, Department of Zoology, University of California, Davis, CA 95616.

Dr. Chen's present address is Dept. of Physics, East China Normal University, Shanghai, PRC.

Dr. Burton's present address is Dept. of Biophysics, King's College, London, England.

Characterization of elliptically polarized light requires the determination of both the ellipticity and the phase. Although measured as distinct quantities, the phase and the ellipticity have the same origin. In the classical model of the interaction of light with matter, the response of electrons in a substance to incident radiation results in the production of induced dipoles. Light that is emitted by these induced dipoles is modified in its amplitude by the magnitude of the polarizability, while its phase is altered by the index of refraction of the material. Because there are constitutive relationships between the index of refraction and the microscopic polarizability, anisotropy in the polarizabilities will be reflected in the measured birefringence. For simple systems, therefore, the measurement of either one of these two quantities would suffice for the complete characterization of the system. For the complex muscle system, even at the level of a single fiber, there are at least two significant components providing measurable optical anisotropy in the electric field amplitudes and in the birefringence (Yeh and Baskin, 1988). These components are the intrinsic contribution and the form contribution. In order to provide an understanding of the relative magnitude of each of these components, one needs to obtain accurate measurements of the fiber diameter, the ellipticity, and the birefringence. Here, we have used a

0006-3495/89/09/595/11 $2.00

previously described (Baskin et al., 1986) method to measure the birefringence and differential field ratio of the diffracted light from single fibers. The use of the diffraction order on which to conduct our measurements renders this technique uniquely suitable to obtaining both the total birefringence and the total differential field ratio in one experiment. Although similar information does exist on the forward transmitted light signal, researchers normally determine only total birefringence from such a measurement (Irving and Peckham, 1986). The fact that there is a strong forward noninteracting signal in these birefringence experiments makes this approach unsuitable for the determination of the typically quite small ellipticity differences occurring in single muscle fibers. On the diffraction order, however, because of the absence of the forward beam, small changes in the state of polarization of light are reflected in the ellipticity of the polarized light, and can indeed be measured.

I. EXPERIMENTAL METHOD

A. Fiber preparation

Single muscle fibers were dissected from the *anterior tibialis* muscle of frog (*Rana pipiens*) in Ringer's solution at low temperature (~6°C), and then put into the skinning solution for ~2 h. The skinning solution[1] contained (millimoles per liter) caffeine (10.0), EGTA (30.0), ATP (5.0), $MgCl_2$ (5.0), TES (60.0), potassium-propionate (100.0), and 0.25% Triton at a pH of 7.1. When the fiber was isolated it was inspected under a dissecting microscope for damage. The fiber was mounted horizontally in a chamber filled with solution at 6°C (see Table 1 for the relaxing, preactivation and activation solution compositions, these solutions are of approximately the same ionic strength [Fabiato and Fabiato, 1979]). The sarcomere length of the fiber could be adjusted and measured by laser diffraction. Tension was measured by an AE80 transducer (Aksjeselskapet Mikro-Elektronikk, Horten, Norway).

To perform the Ca^{++} activation experiment, data are obtained 1.5 min after we changed the solution from relaxing to preactivation and then to activation. We typically performed the activation experiment at two different sarcomere lengths with any given fiber. Initially the fiber was at the resting sarcomere length of 2.2–2.3 μm. After the first activation experiment it was placed into relaxing solution, stretched to a new length and then activated a second time. Data are taken both in the relaxed state and in the activated state. The rigor state is obtained by placing the fiber in a relaxing solution which does not contain CPK, CP, or ATP.

B. Apparatus

Linearly polarized light from a He-Ne laser (model 105-1; Spectra-Physics Inc., Mountain View, CA) operating at 633 nm impinges upon the fiber from below as shown in Fig. 1 *a*. The plane of polarization of this light source is oriented at 45° to the fiber axis, which is the *y*-axis in the laboratory coordinate system. It is imperative that the angle of 45° be held very accurately in order that the projections of the incident field upon the axes parallel and perpendicular to the fiber have the same magnitude. The plane of polarization is finely tunable by a rotating half-wave plate located below the fiber chamber. Absolute angular setting accuracy is better than 0.3°, and all elements of the ellipsometer used to measure that state of polarization are indexed to the same laboratory frame of reference with the same accuracy.

TABLE 1 Composition of solutions used in relaxed-preactivate-activation states

Activation solution II pH 7.1		Pre-active solution II pH 7.1	
TES	60 mM	Caffeine	10 mM
EGTA	15 mM	EGTA	0.1 mM
$MgCl_2$	5 mM	MgCl2	5 mM
Caffeine	10 mM	TES	60 mM
$CaCO_3$	10 mM	K-propionate	55 mM
CPK	1 mg/ml	CPK	1 mg/ml
CP	5 mM	CP	5 mM
ATP	5 mM	ATP	5 mM
Albumin	1 mg/ml	Albumin	1 mg/ml
pCa^{++} 6.28			
Ionic Strength = 108.59 mM		Ionic Strength = 103.4 mM	

Relaxing Solution II pH 7.1	
TES	60 mM
EGTA	15 mM
$MgCl_2$	5 mM
Caffeine	10 mM
CPK	1 mg/ml
CP	5 mM
ATP	5 mM
Albumin	1 mg/ml
Ionic Strength = 106.9 mM	

The laser beam is not focused onto the fiber, thus the uniphase TEM_{00} mode beam has a cross-section (full weight half measure) at the fiber of ~1 mm in diameter. This width assures that a very large number of sarcomeres are involved in producing the diffraction pattern. Indeed, very sharp patterns are observed. Several diffraction orders, both left and right, can be observed when a screen is placed after the fiber. For this work, we restricted our investigations to the first order diffraction pattern, either left or right. The ellipsometer used in these studies consists of a rotating quarter-wave plate, a polarizer, and a photodetector. The quarter-wave plate (Melles Griot, Irvine, CA) is mounted on a platform that rotates upon the drive of a stepping motor (SM). This motor is computer controled thus regulating the size of the step and the dwell time at each step. Upon the end of each 180° rotation, the motor is stepped backward to its original starting position. The repeatability of this setting is better than 0.3°. For these studies, each step rotates the plate by 2°, and the dwell time was set at 2 s. per stop. We used a Glan-Taylor prism (GTP) (Karl Lambrecht Corp., Chicago, IL) for the final analyzing prism with its passing axis set at precisely 0°. The extinction ratio of this device over the diameter of the laser beam is better than 1:100,000. A 633 nm interference filter (F) with 2 nm passband is used to eliminate unwanted light before it reaches the photomultiplier tube (PMT; EMI-Electronics, Ltd., Middlesex, UK). For better stray and scattered light rejection, two variable opening pinhole diaphragms, D1 and D2, are used. The acceptance angle for this system is ~0.5°. The photocounts from the PMT are amplified and pulse-height discriminated using a model 1122 (PARC EG&G Princeton Applied Research, Princeton, NJ) preamp-discriminator before sending the uniform stream of pulses into the dedicated microcomputer

[1]Abbreviations used: ATP, adenosine-5'-triphosphate; C, centigrade; EGTA, ethylene glycol bis-(β-aminoethyl ether) *N,N,N',N'*-tetraacetic acid; CPK, creatine phosphokinase; CP, creatine phosphate.

(Digital Equipment Corp., Boston, MA; LSI 11/23) to be paired with the corresponding quarter-wave plate angle of rotation. The schematic diagram of the ellipsometric system is shown in Fig. 1 *b*.

For the ellipsometric system described in the above paragraph, we have previously derived an expression that relates the intensity of the photoelectric signal to the angle of the rotating quarter-wave plate (Yeh and Pinsky, 1983). This equation is:

$$I_D = 1/2[I_M + Q_M \cos^2 2\theta_Q + U_M \sin 2\theta_Q \cos 2\theta_Q - V_M \sin 2\theta_Q], \quad (1)$$

where I_M, Q_M, U_M, and V_M are the four Stokes elements describing the state of polarization of the muscle fiber. These quantities are in turn related to the measured parameters of elliptically polarized light detected on the diffraction order at an angle θ_D from normal.

$$I_M = I_\parallel \cos^2 \theta_D + I_\perp \quad (2a)$$

$$Q_M = I_\parallel \cos^2 \theta_D - I_\perp \quad (2b)$$

$$U_M = 2I_\parallel I_\perp \cos \theta_D \cos \delta \quad (2c)$$

$$V_M = 2I_\parallel I_\perp \cos \theta_D \sin \delta, \quad (2d)$$

where $I_\parallel$ and $I_\perp$ are the intensities of diffracted light parallel and perpendicular to the fiber axis and δ is that net phase shift between these directions. One notes that the phase shift, δ, is obtainable from the ratio of V_M/U_M, while from the first two relations for I_M and Q_M, the intensities parallel and perpendicular to the fiber are calculated. From the phase angle measurement, $\tan \delta = V_M/U_M$; the total birefringence is then calculated by the equation relating the phase retardation angle, δ (in degrees), to the total birefringence value, Δn_T:

$$\Delta n_T = (\lambda_o \delta)/(360d), \quad (3)$$

where λ_o is the wavelength of light in vacuum, and d is the fiber depth traversed by the light beam.

The small difference in the field amplitudes forced us to evaluate not the ellipticity but the differential field ratio (DFR), defined as

$$r_T \equiv \frac{E_\parallel - E_\perp}{E_\parallel + E_\perp} = \frac{(E_{diff})_\parallel/\cos \theta_D - (E_{diff})_\perp}{(E_{diff})_\parallel/\cos \theta_D + (E_{diff})_\perp}. \quad (4)$$

Here, $(E_{diff})_i$, is each proportional to the product of the effective polarizability and the local field along that direction, and because we are studying the signal on the diffractive pattern, the diffraction angle is θ_D. It is clear that such a ratio measures only the difference in the magnitudes of the diffracted fields and is independent of the incident light beam intensity of the laser source. Because the photodetectors can only sense intensities, the differential field ratio takes on the form

$$r_T = \frac{\sqrt{I_\parallel}/\cos \theta_D - \sqrt{I_\perp}}{\sqrt{I_\parallel}/\cos \theta_D + \sqrt{I_\perp}}, \quad (5)$$

where $\sqrt{I_\parallel} = (E_{diff})_\parallel$ and $\sqrt{I_\perp} = (E_{diff})_\perp$ have been used. Thus both the total birefringence and the DFR value are obtained from a single measurement on the diffraction signal.

For the purpose of converting the phase angle to the total birefringence value, (Eq. 3), the diameter of the fiber is measured by placing a mirror at a 45° angle in the sample chamber. In this way, the depth of the fiber is projected through 90° onto the focal place of the monitoring microscope. Studies by Matsubara et al. (1984) have shown that the lattice spacing between *A* and *I* bands obtained by x-ray diffraction measurements has a direct correspondence with the fiber diameter over sarcomere lengths where there is at least some overlap between the *A* and *I* band filaments. We have used these microscopic measurements of the fiber diameters as reasonable estimates required for determining birefringence. The accuracy of our measurement using a 60x objective and a Filar eyepiece (Baush and Lomb, Rochester, NY) is ~1 μm.

An initial check as to the integrity of the single fiber is made in the following manner. The fiber is scanned along its length for a region which exhibits nearly equal left-right intensity of diffraction for the same order. Data are obtained only from the weaker of the orders, either left or right, in order to minimize Bragg reinforcement related form effects. Ellipsometry measurements are conducted over a range of ~1 mm to insure that the passive fiber has nearly constant δ and r_T values over that 1 mm region. If such a region cannot be found, the fiber is discarded. If such a region is found, care is taken to keep that same region illuminated by the incident light. This is ensured during alteration in sarcomere length by applying equal stretches to each end of the fiber.

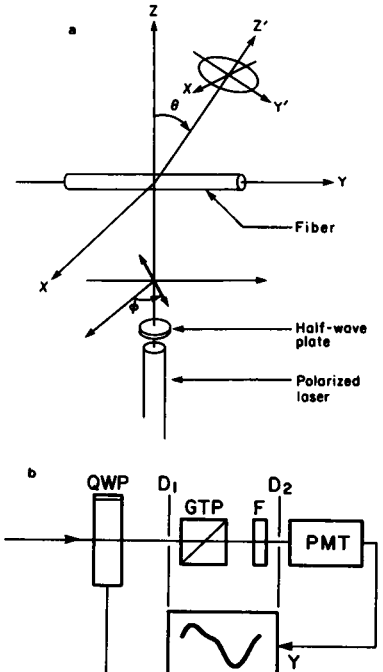

FIGURE 1 (*a*) Schematic diagram of the diffractometer. The diffraction angle θ and the plane of polarization of the incident light, $\phi = 45°$, are indicated. (*b*) Optical ellipsometer using a rotating quarter-wave plate (QWP) is driven by a stepping motor (SM). The light passes through a diaphragm pair, D_1 and D_2, placed on either side of an analyzing polarizer (GTP) and an interference filter *F*. The detector is a photomultiplier tube (PMT).

III. RESULTS

A. Characterizing the relaxed fiber

Sarcomere length dependence of the relaxed skinned fiber:

Because all of the activation studies involve comparing the values of total birefringence and DFR between the

relaxed state and the activated state, we decided to fully characterize this relaxed state. As a muscle is passively stretched, three parameters are measured. First, the diameter of the fiber over a region near the point where the laser beam intersects the fiber is measured. Then the phase shift and DFR are measured using our ellipsometer. Both Δn_T and r_T are determined according to Eqs. 3 and 5. In all cases considered, three measurements are taken at each sarcomere setting and the average value is plotted. Each fiber is measured at 4 to 11 different sarcomere lengths. Birefringence is computed from the phase angle and the fiber thickness as we have previously described (Yeh et al., 1987). Twelve relaxed, skinned fibers were studied. Figs. 2 *a* and *b* represent the normalized sarcomere length dependence of birefringence (Δn_T) and DFR (r_T), respectively. (Fiber diameter was measured at each sarcomere length).

Normalization was carried out in the following fashion: Because of fiber to fiber variabilities the absolute values of Δn_T and r_T differ among the fibers even at the same sarcomere length. We therefore used a reference SL (2.2 μm) and the averaged value of Δn_T and r_T at that SL for the point of normalization. Data from all other fibers were normalized to the value at the reference SL. The sarcomere length dependence of both Δn_T and r_T is internally consistent even though absolute values vary. The single error bar on each figure represents the range of values of all the fibers at that SL before normalization.

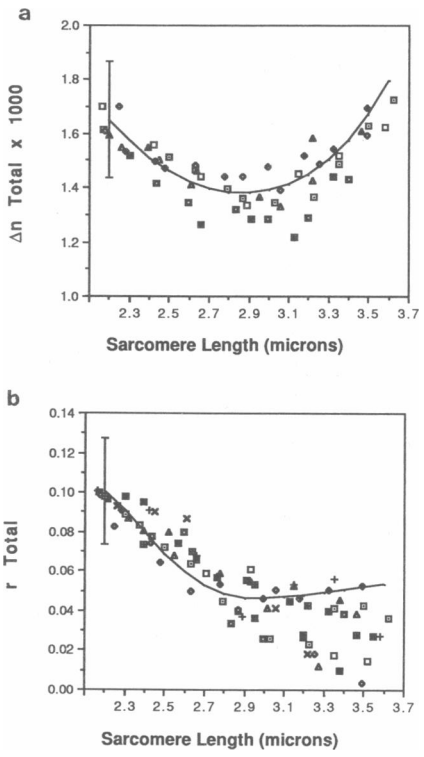

FIGURE 2 (*a*) Total birefringence, Δn_T, for eight skinned fibers, (each symbol is for a different fiber) normalized to average value at a sarcomere length of 2.2 μm. Vertical bar represents range of values. Solid line is based on theory (see Appendix) and model herein presented. (*b*) Total differential field ratio, DFR, r_T, for twelve skinned fibers normalized as in Fig. 2 *a*. Solid line is based on theory and model presented in this paper.

Having performed these normalization studies, we concluded that the data from each fiber exhibited a clear SL dependence. The solid lines represent the SL trends predicted by the new version of our theory (see Appendix). The choice of parameters have been detailed in the Appendix; the indices of refraction and volume fraction assignment are listed in the caption to Fig. 8. In either the skinned fiber or the intact fiber case, one set of parameters is used for both the r_T and Δn_T predictions. Normalization to the experimental parameters at the reference SL was again made. Due to the large number of variables in the theoretical model, we have yet to ascertain the uniqueness of the fit to data. However, we have found that there is great sensitivity in the values of Δn_T and r_T upon S-1 tilt angle variation, but less sensitivity to S-2 tilt changes.

The average absolute value of birefringence of a relaxed fiber at a S.L. of 2.2 μm is 1.60×10^{-3}. This compares with Taylor's (1976) value of 1.67×10^{-3}. The data for both Δn_T and r_T show scatter around the theoretical values as represented by the solid line in each figure. The largest variation occurs in comparing data from different fibers. This is most likely related to the fact that the intensity of the first order line usually varies from fiber to fiber and can vary even among regions of a given fiber. We have previously (Yeh et al., 1980) discussed this phenomena and we believe that it is related to myofibrillar organization (particularly sarcomere skew) that we have shown can vary within a single fiber, leading at times to different intensities of the left and right order lines. Recent index matching studies (unpublished data) have shown that when form contribution to Δn_T and r_T is decreased, the variability along the length of a single fiber dramatically diminishes. We therefore feel that our normalization procedure is justified and leads to a true picture of the variation in Δn_T and r_T with sarcomere length.

Intact relaxed fiber upon sarcomere length change

For these fibers, the isovolumic constraint requires that

$$d = (V_o/\pi SL)^{1/2}, \quad (6)$$

where V_o is the resting sarcomere volume, d is the fiber diameter, and SL is the sarcomere length. This relationship has been verified by our fiber diameter measurements. Since we also measured the diameter after skin-

ning, which is ~10% larger, we conclude that if lattice spacing changes alone were responsible for the changes in Δn_T and r_T, the intact fiber would exhibit a larger total birefringence and a smaller DFR value than the same fiber after skinning. We find, instead (Fig. 3, *a* and *b*), that whereas total birefringence is higher in the intact fiber (~1.7×10^{-3}), the DFR value is also significantly larger than that of the skinned fiber. As in Fig. 2, *a* and *b* the data from individual fiber measurements has been normalized. In both Fig. 3, *a* and *b* normalization has been to the average value at a sarcomere length of 2.45 μm. The vertical bar in each figure represents the range of values at the given sarcomere length. The solid line represents the theoretically determined relationship for SL dependence (see Appendix). The difference in theoretical curves between Figs. 2 and 3 is due to the different diameter-to-SL relationship in the two cases. The data are scattered in both figures. The basis for this is the same as we discussed previously for Fig. 2, *a* and *b*. We further attribute the increase in DFR to the fact that intrinsically anisotropic elements play a major role in developing the observed optical signals (Yeh and Baskin, 1988).

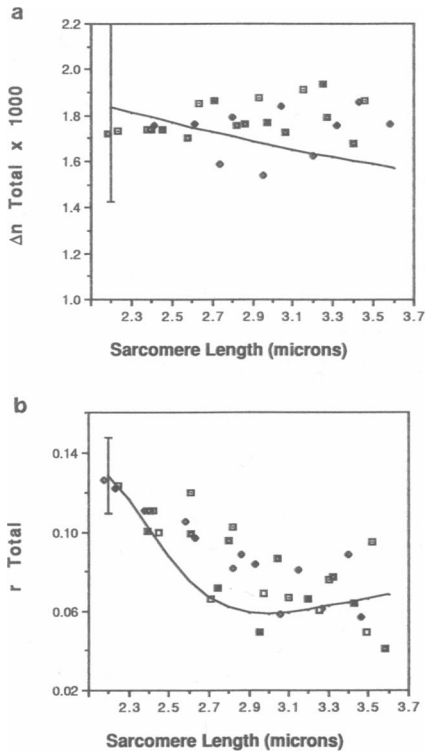

FIGURE 3 (*a*) Total birefringence (Δn_T) for five single, intact fibers plotted as a function of sarcomere length. Values are normalized to the average value at a sarcomere length of 2.4 μm. Vertical line indicates range of values. Solid line is based on theory and model. (*b*) Total differential field ratio (DFR) r_T, for six single, intact fibers plotted as a function of sarcomere length. Values are normalized to average value at a sarcomere length of 2.4 μm. (Vertical line indicates range of values. Solid line is based on theory and model.)

B. Characterizing the activated fiber

Tension measurement vs. sarcomere length

Because the major goal of this investigation is the measurement of the polarization state of diffracted light in an activated, skinned fiber, it is necessary to establish conditions for the repeatable activation of fibers at different sarcomere lengths. We used a calcium concentration that allowed activation at a level ~60% of maximum (pCa = 6.25) throughout these experiments. Under these conditions we measured a tension of 1.31 ± 0.19 kg/cm^2 (mean ± SD) for three samples taken over a sarcomere length range between 2.27 and 2.41 μm.

As sarcomere length was increased (each sarcomere length represents a different fiber), we measured a monotonic decrease in tension (Fig. 4). The solid line corresponds to a least squares fit of the data. This fit has a correlation coefficient of 0.83.

Ca^{++} activation results on Δn_T and r_T

Because solution activation of single fibers results in fiber fatigue, these studies were conducted over a large number of fibers. For each fiber, we initially activated it at a sarcomere length close to the resting length. The fiber was then relaxed and stretched to a second length. At the new length, it was activated for a second time. If a fiber could not sustain the second stretch-activation protocol, then only the data from the first activation was used.

We chose to work at an ionic strength (~100 mM) that in rabbit skinned fibers shows no change in lattice spacing

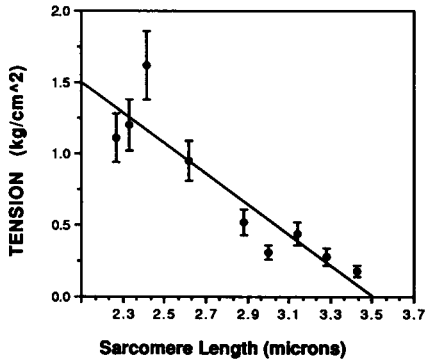

FIGURE 4 Measured active tension for skinned fibers as a function of sarcomere length. Each data point corresponds to the average of three measurements on one fiber. Error bars represent standard deviations. Line represents linear least squares fit with a correlation coefficient, r^2, of 0.831.

upon activation or passage into rigor (Ferenczi et al., 1987). We make the assumption that the same is true for frog muscle skinned fibers at this ionic strength. This assumption was supported by our measurements of fiber diameter. In a study of 18 fibers, held at sarcomere lengths between 2.12 μm and 3.64 μm we observed no diameter change after fiber activation or upon passage into rigor.

Upon activation of a relaxed fiber (Fig. 5 *a*), a small decrease in birefringence was observed at most sarcomere lengths. (Each sarcomere length represents data from a different fiber). The DFR also showed a decrease upon activation of the fiber (Fig. 6 *a*), however this decrease averaged 18% and was larger than that observed for the birefringence change. Both in the case of Δn_T and DFR a decrease was seen at most sarcomere lengths.

Effect of relax to rigor transition on Δn_T and r_T

After placement of a relaxed skinned fiber into rigor, both the value of birefringence (Δn_T) (Fig. 5 *b*) and the value of DFR (R_T) (Fig. 6 *b*) decrease. This decrease is observed at most sarcomere lengths and is similar to that seen upon fiber activation. It is not possible, within the limits of experimental error, to observe any difference in the activation decrease as contrasted with the rigor decrease. It should be noted that there is strong evidence (Cooke et al., 1984; Huxley and Kress, 1985) suggesting that only a fraction of the total crossbridge population is generating tension at any instant. It is equally likely that

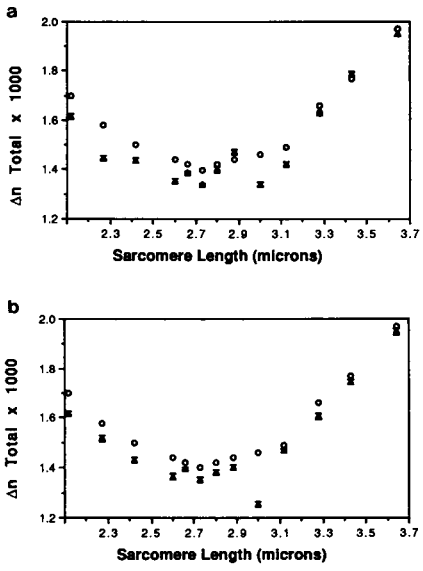

FIGURE 5 (*a*)Birefringence (Δn_T) plotted as a function of sarcomere length for skinned, single fibers. (*a*) Relaxed fiber (O) contrasted with activated fiber (▲). (*b*) Relaxed fiber (O) compared with rigor fiber (▲).

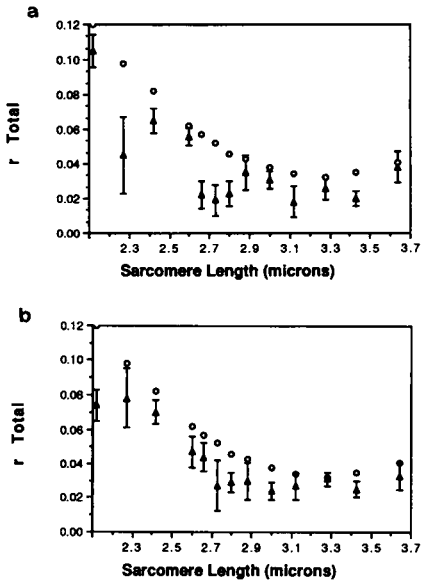

FIGURE 6 Differential Field Ratio (DFR), r_T, plotted as a function of sarcomere length for skinned, single fibers (*a*) Relaxed fiber (O) compared with activated fiber (▲). (*b*) Relaxed fiber (O) compared with rigor fiber (▲). The fibers are represented by a best fit quadratic curve.

crossbridges assume an average position nearer to the actin filaments in the activated (and rigor fibers) than in the relaxed state. The decreases observed in Δn_T and r_T in either activation or rigor, may be due mainly to a more perpendicular attitude (on the average) of either the S-1 or S-2 portion of the cross-bridge. Our results furthermore argue for a similar, average cross-bridge orientation in activated and in rigor fibers. Activation of a skinned fiber would result in an attitudinal change in most cross-bridges even though only a fraction may be generating tension at any one time.

In developing the plots for a change of fiber state from the relaxed to either the rigor or the activated state (Figs. 5 and 6), we used a single representative skinned fiber with its passive stretch behavior as a reference. The data indicating changes of state, to either rigor or activation, are then plotted as changes from that reference relaxed fiber state. Again the purpose is to show that taking away the fiber-to-fiber variability, there exist trends that are repeatable and can be interpreted within the context of crossbridge orientation changes.

IV. DISCUSSION

This investigation has established the following: (*a*) Passive stretch of a skinned fiber in its relaxed state results in a large decrease in the DFR value, r_T, as sarcomere length is increased. The total birefringence Δn_T also shows a

dependence on sarcomere length, showing higher values at short and long sarcomere lengths and a minimum value at a SL of ~2.9 μm. (*b*) Passive stretch of an intact fiber produced a smaller change in r_T than was observed in a skinned fiber, and no significant change in Δn_T. (*c*) Fiber activation results in a decrease in r_T and Δn_T at most sarcomere lengths. (*d*) The percentage of decrease is smaller at longer sarcomere lengths. Passage of a relaxed fiber into rigor results in changes in Δn_T and r_T similar to those seen after fiber activation. (*e*) We have attempted to correlate the experimental results with a theoretical formulation that considers average crossbridge position in the different fiber states.

Variation in the values of birefringence, (Δn_T), and DFR, (r_T).

The average value of birefringence (Δn_T) in a single, skinned frog muscle fiber was 1.60×10^{-3} (SL = 2.2 μm) in agreement with an earlier study of Taylor (1976). This value was dependent upon sarcomere length, showing first a decrease and then an increase with a minimum value at a sarcomere length of ~2.90 μm.

In both intact and skinned fibers the value of the DFR, (r_T), shows a decrease as sarcomere length is increased. The magnitude of r_T decreasing during stretch from a sarcomere length of 2.3 μm to a sarcomere length of ~3.0 μm and then assuming a minimum value. Upon activation of a skinned fiber, the magnitude of r_T decreases and this decrease is observed at most sarcomere lengths.

Lattice spacing changes in intact and skinned fibers

The work of Matsubara and Elliott (1972) provides us with a measurement of the change in $d_{1,0}$ (nm) spacing as an intact fiber is stretched (Fig. 7). Also plotted on the same figure are the data of Higuchi and Umazume (1986) showing the change in $d_{1,0}$ in a skinned fiber. Note that due to the isovolumic nature of the intact fiber, the value of $d_{1,0}$ is inversely proportional to the square root of the sarcomere length over the range from 2.2 μm to ~3.6 μm. The situation is different, however, in the chemically skinned fiber. In this case the muscle is clearly not isovolumic. There is little change in $d_{1,0}$ in the sarcomere length range from 2.2 μm to 3.0 μm; past a sarcomere length of 3.0 μm a nearly linear change in $d_{1,0}$ is observed as sarcomere length is increased to 3.6 μm. Thus, the lattice spacing of an intact fiber shows a different relationship to sarcomere length than the lattice spacing of a skinned fiber.

In the study by Matsubara and Elliott (1972) the ionic strength was lowered to 0.09 M (mechanically skinned frog fibers). At this ionic strength almost no change in lattice spacing was observed as sarcomere length was varied between 2.15 μm and 3.40 μm. They explained these results on the assumption that the filament lattice was near to its structural limit. The reduction in ionic strength is believed to cause an increase in the electrostatic repulsive force by reducing the counter-ions in the interfilament space. These results are consistent with our measurements of fiber diameter even though our system is a chemically skinned fiber, and explain why no change in fiber diameter was observed upon fiber activation or passage into rigor.

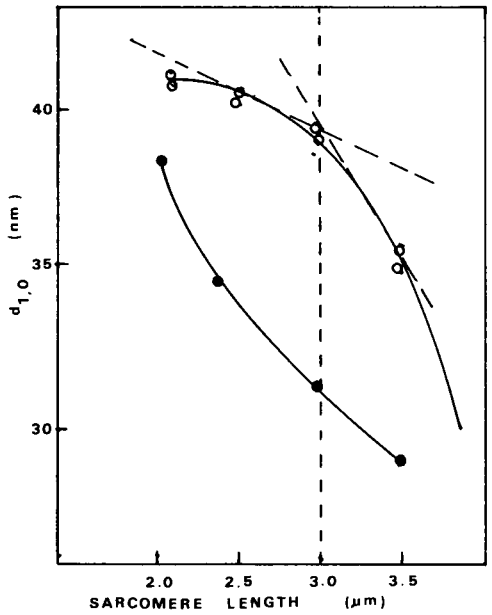

FIGURE 7 Variation in $d_{1,0}$ spacing as a function of sarcomere length. (O) Chemically skinned fiber, (●) intact fiber. (Skinned fiber data reproduced from the work of Higuchi and Umazume, (1986); intact fiber data reproduced from the work of Matsubara and Elliot [1972]).

Passive stretch of the intact fiber

In the intact fiber, which is isovolumic upon change in sarcomere length, there is no change in the total volume fraction upon stretch. However, two factors must be considered. First, orientational constraints of the S-1 and S-2 moieties are present in the overlap region, even though the nature of the constraint is different because of the isovolumic criterion. Secondly, as the fiber is stretched the ratio $[I_{1,1}/I_{1,0}]$ (x-ray diffraction) decreases as the thin filaments lose register and are pulled out of the *A*-band. The loss of register of the thin filaments (and their resulting increased randomness) leads to a decrease in shape related form anisotropy, and is consistent with decreases in the value of r_T and Δn_T.

Modeling of cross-bridge induced changes in the ellipsometry spectrum

In a previous study (Yeh and Baskin, 1988), theoretical expressions for the total birefringence, Δn_T, and the differential field ratio, r_T, were derived. In that study, the sarcomere was modeled as a simplified two-region repeating unit, *A*-band and *I*-band. The *A*-band index of refraction was assumed to be optically anisotropic while the *I*-band was maintained as an optically isotropic region. Differences of the orientation of cross-bridge elements in the overlap region and those in the nonoverlap region were modeled by different tilt angles of the S-2 elements leading to a changing intrinsic anisotropy contribution. The orientation changes of S-1 moieties were modeled by the increase in the rotundness of the indicial ellipsoid for the *A*-band as a result of the angle of tilt of S-1 changes. Since that publication, we have improved upon that model by incorporating two additional features: (*a*) The sarcomere is now divided into three sections: Nonoverlapping region of the *A*-band, overlapping region of the *A*-band, and the *I*-band. (*b*) The orientation changes of the S-1 moieties are modeled in a manner similar to that developed by Carlson et al. (1987). The S-1 elements now can assume distinct angles of tilt when they are within the overlap region; they assume an average orientation in the nonoverlap region parallel to the fiber axis. Using this new model we shall analyze the following states of the sarcomere.

The chemically skinned fiber in its relaxed state

As a chemically skinned fiber is passively stretched, cross-bridges are pulled out of overlap with the thin (actin) filaments. In the present form of our theory (see Appendix), we weight the local field in each of three regions by the partial specific volume for that region. The change in the local field upon an increase in the sarcomere length results in a net decrease in the values of Δn_T and r_T. This is reversed at long sarcomere lengths due to lattice spacing changes. It is important to emphasize that the changes in partial specific volume that we are referring to here are caused by changes in filament overlap. Lattice spacing changes can also result in partial specific volume changes and these we discuss next.

Countering the effects of partial specific volume changes in each region, the skinned fiber will develop a different contribution to ellipsometry changes upon further stretch. Once past a sarcomere length of 3.0 μm where the number of overlapping cross-bridges becomes quite small, the lattice spacing of these skinned fibers change rather dramatically (Higuchi and Umazume, 1986). This change in lattice spacing will result in corresponding changes in the volume fractions of the elements of skinned fibers, which are not isovolumic. The increasing volume fraction will lead to an increasing contribution of form birefringence and form DFR at these longer sarcomere lengths. Thus the total birefringence and DFR will both experience the effect of this second contribution, leading to an apparent biphasic behavior.

Changes of state: relax-activate-rigor

We have made the following assumptions for the orientations of both S-1 and S-2 in the relaxed or resting state of the fiber. These are: for the overlapping region, S-1 is assumed to have a tilt angle of its major axis with respect to the fiber axis, $\theta_1 = 30°$. This assumption is due to the work of Cantino and Squire (1986) where, based on electron microscopy studies, these authors developed a model with θ_1 angle between 20° and 40°. We thus chose the mid-point in our model representation of θ_1. The S-2 angle, θ_2, in the resting state is assumed to be 0°. In the nonoverlapping zone, S-2 orientation θ_2 is still assumed to be 0°, but the orientation of the S-1 moieties is much more random, leading to an averaged $\langle(\sin\theta_1)^2\rangle = 0.5$.

For the activation state, we have chosen an angle θ_1 which is intermediate between that of the resting value and the rigor value of 68°, determined by Thomas and Cooke (1980) using spin probes. Thus in the overlapping region, the value of $\theta_1 = 50°$ is taken. Because there is more S-1 tilt in this state, we assumed that the angle of tilt for S-2, θ_2, must follow correspondingly. We used a value of 10° for θ_2 in the overlapping region. As before, no change is assumed for those cross-bridges in the nonoverlapping region.

The rigor state is modeled by the following overlapping region parameters: $\theta_1 = 70°$, consistent with the value of Thomas and Cooke. Here, the S-2 tilt angle, θ_2, must further increase, and we used a value of 15°. The nonoverlapping region is assumed to retain the original resting values as before.

With only these changes in S-1 and S-2 of orientation, we find that the change in both the total birefringence and total *r*-value can be as high as 10 to 20%. In all cases, the resting fiber had the largest values of both of these quantities, the activation state assumed the intermediate values, and the rigor state had the lowest values (Fig. 8). These changes are similar to the experimental results we obtained for the skinned fiber, although the experimental data are not accurate enough to resolve a difference between the signal of the activated state from that of the rigor state. (We have not considered the possibility of a local phase transition in the LMM-S-2 hinge region [Ueno and Harrington, 1986]. Such a transition should

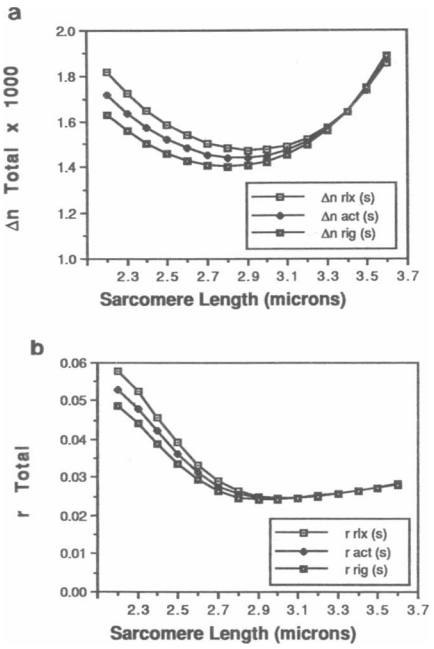

FIGURE 8 Birefringence (Δn_T), (*a*), and Differential Field Ratio (r_T), (*b*) plotted as a function of sarcomere length. Plots are based on theoretically derived equations (see Appendix). The values used in constructing these plots are $n_{A\parallel} = 1.535$, $n_{A\perp} = 1.525$, $n_1 = 1.515$, $n_i = 1.350$, $f_{A_o} = 0.040$, $f_{S\text{-}1_o} = 0.021$, and $f_{1_o} = 0.040$.

	Overlap	Nonoverlap
Relax S-1	30°	$\langle(\text{Sin}\theta_1)^2\rangle = 0.5$
S-2	0°	0°
Activated S-1	50°	$\langle(\text{Sin}\theta_1)^2\rangle = 0.5$
S-2	10°	0°
Rigor S-1	70°	$(\text{Sin}\theta_1)^2 = 0.5$
S-2	15°	0°

Symbols are □ = Relax; ■ = Rigor; ◆ = Activate.

show up in our experimental results but it was not considered in our analysis).

APPENDIX

Two new features have been added modifying the original theory of Yeh and Baskin (1988), which provided an analysis of the optical diffraction ellipsometry pattern from single fibers of muscle. First, we deal more specifically with the overlapping region between the thick and the thin filaments. This overlap region is now considered a variable with sarcomere length dependence and possesses its own optical characteristics. Second, the S-1 contribution to optical ellipsometry has been separated from that of the total *A*-band. In this manner, the specific orientation of the S-1's can be independently assigned. The basis of this second feature is the work of Carlson et al. (1987). We discuss each of these new aspects in this appendix.

(a) The sarcomere elements considered. The basic half-sarcomere is divided into three sections: (*a*) the nonoverlapping region where the myosin rod, S-2 and S-1 can exist but there is no thin filament contribution; (*b*) an overlapping region where rod, S-2, S-1, and *f*-actin all can exist; and (*c*) the I-band region where only *f*-actin and *Z*-material is considered. Both these two entities are considered optically isotropic, as are the S-1 moieties. Fig. A1 is a representation of the spatial distances of these regions.

Because the total sarcomere distance is given by an independent variable, SL, the half-sarcomere length is given by SL/2. The total *A*-band has a length of z_A, which we have set at 1.6 μm; each of the *f*-actin filament is assigned a length of z_I(= 1.0 μm). There are two z_I regions within a sarcomere. The overlap region extends from the point where the *f*-actin starts to overlap the *A*-band and terminates at the variable point $x/2$. The value of x is linearly proportional to the sarcomere length, SL, by the relation

$$(x/2) = (\text{SL}/2) - z_I. \tag{A1}$$

Thus, when SL = 3.6 μm, then $x = 1.6\ \mu\text{m} = z_A$. On the other end, when SL = 2.2 μm, then $x = 0.2\ \mu\text{m}$. The three sections that we shall consider to be distinct will be:

Nonoverlapping region: $x/2$
Overlapping region: $(z_A - x)/2$
I-band region: $(\text{SL} - z_A)2$.

This material distribution will lead to Fourier decomposition, and the contributions of each region towards each of the diffraction orders is then specified.

(b) Volume fraction assignments. The volume fraction assignment can only be made for a well-defined state of the fiber. We considered the resting state to be the reference state of the fiber with a resting length of 2.2 μm. The summarized data of elemental frog muscle content found in Bagshaw (1982) served as the basic reference for volume fraction assignments. The content of other proteins including the connective molecules such as titin and nebulin is estimated from Yates and Geaver (1983).

$f_{A_o} = 0.040$, including LLM's, S-2's, and titin. This region is considered to be optically anisotropic.

$f_{S-1_o} = 0.021$, for the S-1 moieties alone, here assumed to be optically isotropic.

$f_{1_o} = 0.040$, including *f*-actin, TM and Tn as well as a volume fraction of 0.01 for isotropic *Z*-band material and an added 0.005 for nebulin. This entire region is assumed to be optically isotropic.

It is important to note that the volume fraction will change depending on what is done to the fiber. For example, if the fiber is skinned, there is an immediate expansion of the fiber diameter, while the amount of fiber element is not increased. Furthermore, the stretch of the skinned fiber does not keep it isovolumic, thus, the volume fraction will be changing

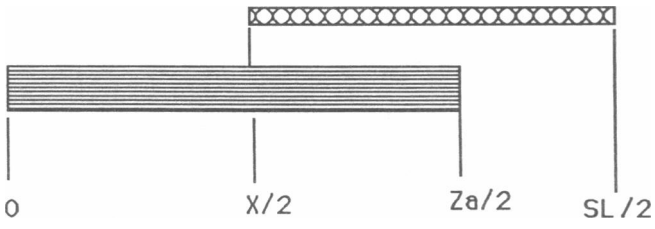

FIGURE A-1 Schematic representation of the half-sarcomere. The overlapping region is from $X/2$ to $Z_a/2$.

with SL in this case. The fiber in intact state, on the other hand, will have isovolumic behavior, thus the volume fractions will not change upon stretch.

Volume fraction as we have defined up to now only relate to the total contributions, not the sectional contributions as we divide the half-sarcomere up into three sections. Thus, we need to assign the partial volume fractions of each of these elements in these sections:

(*a*) Nonoverlap region:

$$\begin{aligned} f_{\text{Anol}} &= f_{\text{Ao}}x/z_{\text{A}}; \\ f_{\text{S-1nol}} &= f_{\text{S-1o}}x/z_{\text{A}} \\ f_{\text{Inol}} &= 1 - f_{\text{Anol}} - f_{\text{S-1nol}} \end{aligned} \tag{A2a}$$

(*b*) Overlap region:

$$\begin{aligned} f_{\text{Aol}} &= f_{\text{Ao}}(z_{\text{A}} - x)/z_{\text{A}} \\ f_{\text{S-1ol}} &= f_{\text{S-1o}}(z_{\text{A}} - x)/z_{\text{A}} \\ f_{\text{Iol}} &= f_{\text{Io}}(z_{\text{A}} - x)/(\text{SL-}x) \\ f_{\text{1ol}} &= 1 - f_{\text{Aol}} - f_{\text{S-1ol}} - f_{\text{Iol}} \end{aligned} \tag{A2b}$$

(*c*) I-band:

$$\begin{aligned} f_{\text{I}} &= f_{\text{Io}}(\text{SL} - z_{\text{A}})/(\text{SL} - x) \\ f_{\text{1I}} &= 1 - f_{\text{I}}. \end{aligned} \tag{A2c}$$

The test of the validity of this apportionment lies with the fact that if we sum up the partial volume fractions of each of the components, we should get the total volume fractions. This is indeed true for all partials including the fact that $f_{\text{1T}} = 1 - (f_{\text{AT}} + f_{\text{S-1T}} + f_{\text{IT}}) = 1 - (f_{\text{Ao}} + f_{\text{S-1o}} + f_{\text{Io}})$.

(c) The use of the Bragg-Pippard result. We have used the local field correction developed by Bragg and Pippard (1953). This is an approximation where a volume fraction of elements contribute to the local field within a dielectric ellipsoid in a manner that the shape of the ellipsoid is accounted for. In the present situation, we have three different elements: *A*-band matter minus S-1, S-1 alone, and *I*-band matter. Both *A*-band and *I*-band matter without S-1 can be considered very long rods, and the values for the depolarization factors, $L_{\|}$ and $L_{\perp}$, in these regions are but small departures from 0.0 and 0.5, respectively. Linear departures as a function of effective axial ratio has been assumed, as was done in the previous work (Yeh and Baskin, 1988). For the S-1 moieties, the most commonly acceptable estimate for the shape is that of a hydrated prolate ellipsoid with an axial ratio nearly 3.0 or 3.5 (Mendelson and Wilson, 1987, Ludescher et al., 1987). Using a value of 3.0, we find from Stoner (1945) that the depolarization values are $\sim L_{\|} = 0.08$ and $L_{\perp} = 0.45$. The local field will be given by

$$E_{im} = E_o/\{1 + [(\epsilon_{im} - \epsilon_1)/\epsilon_1]L_{im}\} \cdot i = \{\|, \perp\}; m = \{A, S\text{-}1, I\}, \tag{A3}$$

where each region and each component will have its contribution. Even though Bragg and Pippard's work does not specify the spatial banding of the dispersed elements of a particular shape, we have imposed that as an additional requirement to mimmick the sarcomere more realistically.

The S-1 contribution in this local field analysis has to take into account of the different orientational attitudes of the axis of the S-1 with respect to the field. For well-defined angles, an orthogonal coordinate transformation similar to that used in our earlier analysis of the S-2 orientation (Yeh and Baskin, 1987), is used. For random orientation of the elements, the effective fields are subsequently angularly averaged over all space. This approach is identical to those invoked by Carlson et al. (1987).

(d) Regional E. D. and ϵ. The idea of this approach is that within each of the regions, there will be partial contributions from all the existing elements. We develop the general electric field, *E*, in each region as the summation of the component parts each weighed by the specific partial volume fraction. This expression is given by

$$E_{iR} = \Sigma_m f_m E_{im} \quad \text{R} = \{\text{NOL, OL, I}\}. \tag{A4}$$

The local *D* field is likewise obtained. In general, the *D* field is related to the *E* field by the regional local dielectric constant ϵ_{im} of each of the parts. Thus, the equation describing the components of *D* field is given by

$$D_{iR} = \Sigma_m \epsilon_{im} f_m E_{im} \tag{A5}$$

From these two equations, we find the regional dielectric constant by the simple relation

$$\epsilon_{iR} = D_{iR}/E_{iR}. \tag{A6}$$

(e) Weighting of the regions in diffraction. The overlapping elements now constitute a complex grating where the periodicity is the sarcomere length SL. We perform the standard Fourier decomposition and obtain the expressions for the contribution of the different regions towards the diffraction patterns. These are

$$\epsilon_{i0} = (2/\text{j})[\epsilon_{i\text{nol}}x + \epsilon_{i\text{ol}}(z_{\text{A}} - x) + \epsilon_{i1}(\text{SL-}z_{\text{A}})] \tag{A7}$$

$$\epsilon_{ij} = (1/\text{SL})\,[(\epsilon_{i\text{nol}} - \epsilon_{i\text{ol}}) \sin(\pi jx/\text{SL}) + (\epsilon_{i\text{ol}} - \epsilon_{i1}) \sin(\pi jz_{\text{A}}/\text{SL})]. \tag{A8}$$

We now make the assumption that the same local character for the dielectric constant is valid for the local scattered field intensities. That is,

$$(E_{\text{sc}})_{iR} = (\epsilon_{iR} - \epsilon_1)E_{iR}. \tag{A9}$$

Thus we are assuming that the contribution at a particular diffraction order comes from the field contributions which are local in character. The local dielectric constant and the local exciting field together are responsible for the magnitude of the local scattered field. The expressions for the scattered field from each of the *j*th order of diffraction then become:

$$E_{\text{scij}} = (1/\text{SL})\,[(E_{\text{sc}_{i\text{nol}}} - E_{\text{sc}_{i\text{ol}}}) \sin(\pi jx/\text{SL}) + (E_{\text{sc}_{i\text{ol}}} - E_{\text{sc}_{i1}}) \sin(\pi jz_A/\text{SL})]\,. \tag{A10}$$

We have the calculations of the birefringence and differential field ratio:

$$n_{ij}^2 = [\epsilon_{i0} + \epsilon_{\text{ij}}] \tag{A11}$$

and

$$(\Delta n)_j + (n_{\|} - n_{\perp})\text{j}\,; \tag{A12}$$

the differential field ratio, *r*, is given by

$$r_{\text{j}} = (E_{\text{sc}_{\|j}} - E_{\text{sc}_{\perp j}})/(E_{\text{sc}_{\|j}} + E_{\text{sc}_{\perp j}}) \tag{A13}$$

These two quantities, Eqs. A12 and A13, are then plotted as a function of the sarcomere length.

The authors are grateful for the expert fiber preparations obtained by Ms. Quan You Li.

This work is supported in part by a Grant from the National Institutes of Health to Y. Yeh and R. J. Baskin (AR-26817).

J. S. Chen was a visiting scholar from the People's Republic of China.

Received for publication 23 August 1988 and in final form 25 May 1989.

REFERENCES

Bagshaw, C. R. 1982. Muscle Contraction. Chapman and Hall, London. p 76.

Baskin, R. J., Y. Yeh, K. Burton, J. S. Chen, and M. Jones. 1986. Optical depolarization changes in single, skinned muscle fibers. *Biophys. J.* 50:63–74.

Bragg, W. L., and A. B. Pippard. 1953. The form birefringence of macromolecules. *Acta. Crystallorg.* 6:865–867.

Cantino, M., and J. Squire. 1986. Resting myosin cross-bridge configuration in frog muscle thick filaments. *J. Cell Biol.* 102:610–618

Carlson, F. D., R. C. Haskell, and P. S. Blank. 1987. A Model of the form birefringence properties of muscle. *Biophys. J.* 51:471a. (Abstr.)

Cooke, R., M. S. Crowder, C. H. Wendt, V. A. Barnett, and D. D. Thomas. 1984. Muscle crossbridges: Do they rotate? *In* Contractile Mechanisms in Muscle. G. H. Pollack and H. Sugi, editors. Plenum Publishing Corp., New York. pp 413–423.

Fabiato, A., and F. Fabiato. 1979. Calculator programs for computing the composition of the solutions containing multiple metals and ligands used for experiments in skinned muscle cells. *J. Physiol. (Paris).* 75:463–505.

Ferenczi, M. A., R. S. Goody, M. Irving, Y. Maeda, M. Peckham, K. J. V. Poole, and G. Rapp. 1987. Time-resolved measurements of filament lattice spacing in rabbit psoas muscle fibers following rapid photogeneration of ATP from caged-ATP. *Biophys. J.* 51:470a. (Abstr.)

Higuchi, H., and Y. Umazume. 1986. Lattice shrinkage with increasing resting tension in stretched, single skinned fibers of frog muscle. Biophys. J. 50:385–389.

Huxley, H. E., and M. Kress. 1985. Crossbridge behaviour during muscle contraction. *J. Muscle Res. Cell Motil.* 6:153–161.

Irving, M., and M. Peckham. 1986. Birefringence as a probe of crossbridge orientation in demembranated muscle fibers of frog and rabbit. *J. Physiol. (Lond.).* 377:95P.

Ludescher, R. D., T. M. Eads, and D. D. Thomas. 1987. Triplet anisotropy studies of restricted rotational motion in myosin monomers and filaments. *In* Optical Studies of Muscle Cross-Bridges. R. J. Baskin and Y. Yeh, editors. CRC Press, Boca Raton, FL. pp 33–66.

Matsubara, I., and G. F. Elliott. 1972. X-ray diffraction studies on skinned single fibers of frog skeletal muscle. *J. Mol. Biol.* 72:657–669.

Matsubara, I., Y. E. Goldman, and R. M. Simmons. 1984. Changes in the lateral filament spacing of skinned muscle fibres when cross-bridges attach. *J. Mol. Biol.* 173:15–33.

Mendelson, R., and M. G. A. Wilson. 1987. Fluorescence polarization studies of myosin and muscle cross-bridges. *In* Optical Studies of Muscle Cross-Bridges. R. J. Baskin and Y. Yeh, editors. CRC Press, Boca Raton, FL. pp 67–98.

Stoner, E. C. 1945. The demagnetizing factors for ellipsoids. *Phil. Mag.* 36:803–821.

Thomas, D. D., and R. Cooke. 1980. Orientation of spin-labeled myosin heads in glycerinated muscle fibers. *Biophys. J.* 32:891–906.

Ueno, H., and W. F. Harrington. 1986. Local melting in the subfragment-2 region of myosin in activated muscle and its correlation with contractile force. *J. Mol. Biol.* 190:69–82.

Yates, L. D., and M. L. Greaser. 1983. Quantitative determination of myosin and actin in rabbit skeletal muscle. *J. Mol. Biol.* 168:123–141.

Yeh, Y., and R. J. Baskin. 1987. Optical ellipsometry studies on the diffracted orders of single fibers from skeletal muscles. *In* Optical Studies of Muscle Cross-Bridges. R. J. Baskin and Y. Yeh, editors. CRC Press, Boca Raton, FL. pp. 123–148.

Yeh, Y., R. J. Baskin, K. Burton, and J. S. Chen. 1987. Optical ellipsometry on the diffraction order of skinned fibers. Ph induced rigor effects. *Biophys. J.* 51:439–447.

Yeh, Y., and R. J. Baskin. 1988. Theory of optical ellipsometric measurements from muscle diffraction studies. *Biophys. J.* 54:205–218.

Yeh, Y., R. J. Baskin, R. L. Lieber, and K. P. Roos. 1980. Theory of light diffraction by single skeletal muscle fibers. *Biophys. J.* 29:509–522.

Yeh, Y., and B. G. Pinsky. 1983. Optical polarization properties of the diffraction spectra from single muscle fibers of skeletal muscle. *Biophys. J.* 44:83–90.